ETH zürich

ETH Library

Nuclear Reprocessing Tracers Illuminate Flow Features and Connectivity Between the Arctic and Subpolar North Atlantic Oceans

Journal Article

Author(s):
Casacuberta, Núria; Smith, John N.

Publication date:
2023-01

Permanent link:
https://doi.org/10.3929/ethz-b-000585879

Rights / license:
Creative Commons Attribution 4.0 International

Originally published in:
Annual Review of Marine Science 15, https://doi.org/10.1146/annurev-marine-032122-112413

This page was generated automatically upon download from the ETH Zurich Research Collection.
For more information, please consult the Terms of use.

Annu. Rev. Mar. Sci. 2023.15:203-221. Downloaded from www.annualreviews.org
Access provided by ETH- Zurich on 07/24/23. See copyright for approved use.

ANNUAL REVIEWS

Annual Review of Marine Science

Nuclear Reprocessing Tracers Illuminate Flow Features and Connectivity Between the Arctic and Subpolar North Atlantic Oceans

Núria Casacuberta[1] and John N. Smith[2]

[1]Institute of Biogeochemistry and Pollutant Dynamics, Department of Environmental Systems Science, and Laboratory of Ion Beam Physics, ETH Zürich, Zürich, Switzerland; email: nuria.casacubertaarola@usys.ethz.ch

[2]Bedford Institute of Oceanography, Fisheries and Oceans Canada, Dartmouth, Nova Scotia, Canada; email: john.smith@dfo-mpo.gc.ca

ANNUAL REVIEWS CONNECT

www.annualreviews.org

- Download figures
- Navigate cited references
- Keyword search
- Explore related articles
- Share via email or social media

Annu. Rev. Mar. Sci. 2023. 15:203–21

First published as a Review in Advance on September 2, 2022

The *Annual Review of Marine Science* is online at marine.annualreviews.org

https://doi.org/10.1146/annurev-marine-032122-112413

Copyright © 2023 by the author(s). This work is licensed under a Creative Commons Attribution 4.0 International License, which permits unrestricted use, distribution, and reproduction in any medium, provided the original author and source are credited. See credit lines of images or other third-party material in this article for license information.

OPEN ACCESS CC BY

Keywords

tracer, Arctic, Atlantic, circulation, transit time distribution, ^{129}I

Abstract

Releases of anthropogenic radionuclides from European nuclear fuel reprocessing plants enter the surface circulation of the high-latitude North Atlantic and are transported northward into the Arctic Ocean and southward from the Nordic Seas into the deep North Atlantic, thereby providing tracers of water circulation, mixing, ventilation, and deep-water formation. Early tracer studies focused on ^{137}Cs, which revealed some of the first significant insights into the Arctic Ocean circulation, while more recent work has benefited from advances in accelerator mass spectrometry to enable the measurement of the conservative, long-lived radionuclide tracers ^{129}I and ^{236}U. The latest studies of these tracers, supported by simulations using the North Atlantic–Arctic Ocean–Sea Ice Model (NAOSIM) and enhanced by the use of transit time distributions to more precisely accommodate mixing, have provided a rich inventory of transport data for circulation in the Arctic and North Atlantic Oceans that are of great importance to global thermohaline circulation and climate.

Annu. Rev. Mar. Sci. 2023.15:203-221. Downloaded from www.annualreviews.org
Access provided by ETH- Zurich on 07/24/23. See copyright for approved use.

OCEAN WARMING AND TRANSIENT TRACERS IN THE ARCTIC AND SUBPOLAR NORTH ATLANTIC OCEANS

The Changing Arctic and Subpolar North Atlantic Oceans

Climate change is currently triggering profound changes in the marine environment, and the consequences have become readily apparent in the Arctic and subpolar North Atlantic Oceans. On September 15, 2020, Arctic sea ice reached its likely minimum extent for that year (NASA 2022), the second lowest in the satellite record after 2012, which suggests that the upward trend in percentage of sea ice loss (−13.4% per decade for 1979–2020) is even greater than expected from the output of most climate models (Meredith et al. 2019). There are several reasons for the sea ice mass loss. One is the solar-induced heating of the ocean surface mixed layer (SML) as a result of the increased northward heat transport in the atmosphere (Carmack et al. 2015). A second major heat flux accompanies the advection of warm Atlantic Water (AW) through Fram Strait and the Barents Sea into the Nansen Basin (**Figure 1*a***), where the separate branches are transformed through mixing and modification and undergo cyclonic circulation at intermediate water depths of approximately 200–800 m, generally following the bathymetric contours of the Arctic basins (Polyakov et al. 2017, Rudels 2009). While AW represents approximately 90% of the total inflow into the Arctic Ocean, additional heat accompanies both the ∼10% of Pacific Water (PW) that enters through the Bering Strait (**Figure 1*a***) and the surface fresh waters from runoff and precipitation (∼1%) (Woodgate 2013). Inextricably linked to Arctic warming and sea ice loss are the accumulation and storage of fresh water in the Arctic Ocean in addition to the mechanisms and pathways governing its eventual transport to lower latitudes. Although advances have been made in regional observations of AW and freshwater circulation in the Arctic Ocean, the basin-wide structure and pathways are variable, and future responses to an altered Arctic climate are difficult to predict (Timmermans & Marshall 2020).

While the Arctic Ocean is undergoing unprecedented summer sea ice loss and surface warming at a rate of three times the global average (Cao et al. 2017, Timmermans & Marshall 2020), the consequences extend to global-scale storage and cycling of heat, fresh water, carbon, and other climatically and ecologically important properties (Meredith et al. 2019). According to climate model simulations, one of the consequences of the sea ice retreat and changes in Arctic Ocean circulation will be the weakening of one of the engines that drive the global ocean motion: the Atlantic Meridional Overturning Circulation (AMOC) (Sevellec et al. 2017, Srokosz & Bryden 2015). The AMOC connects northward-flowing warm waters and southward-flowing cold waters (**Figure 1*a***) across all latitudes, with the link between northward- and southward-flowing waters maintained through heat loss to the atmosphere and associated water mass transformation at high latitudes (Frajka-Williams et al. 2019). The subpolar North Atlantic, in particular, hosts several formation regions for intermediate- and deep-water masses (**Figure 1*a***). They constitute the northern loop of the AMOC and connect the warm and saline near-surface waters imported from the subtropics via the Gulf Stream and North Atlantic Current to the cold and deep returning flows that constitute the lower limb of the AMOC. Three main deep-water masses are formed in the subpolar North Atlantic as a consequence of heat loss: Denmark Strait Overflow Water, which is the densest contribution to the North Atlantic Deep Water (Jochumsen et al. 2015); Iceland–Scotland Overflow Water; and Labrador Sea Water (e.g., Kieke & Yashayaev 2015). These waters transport surface-ocean properties, including oxygen, heat, fresh water, and anthropogenic carbon, down to deeper layers, thereby ventilating the interior ocean and playing an important role in the mechanisms regulating global climate (Frajka-Williams et al. 2019, Khatiwala et al. 2013, Rhein et al. 2015). The extent to which anthropogenically induced climate change is impacting

Annu. Rev. Mar. Sci. 2023.15:203-221. Downloaded from www.annualreviews.org
Access provided by ETH- Zurich on 07/24/23. See copyright for approved use.

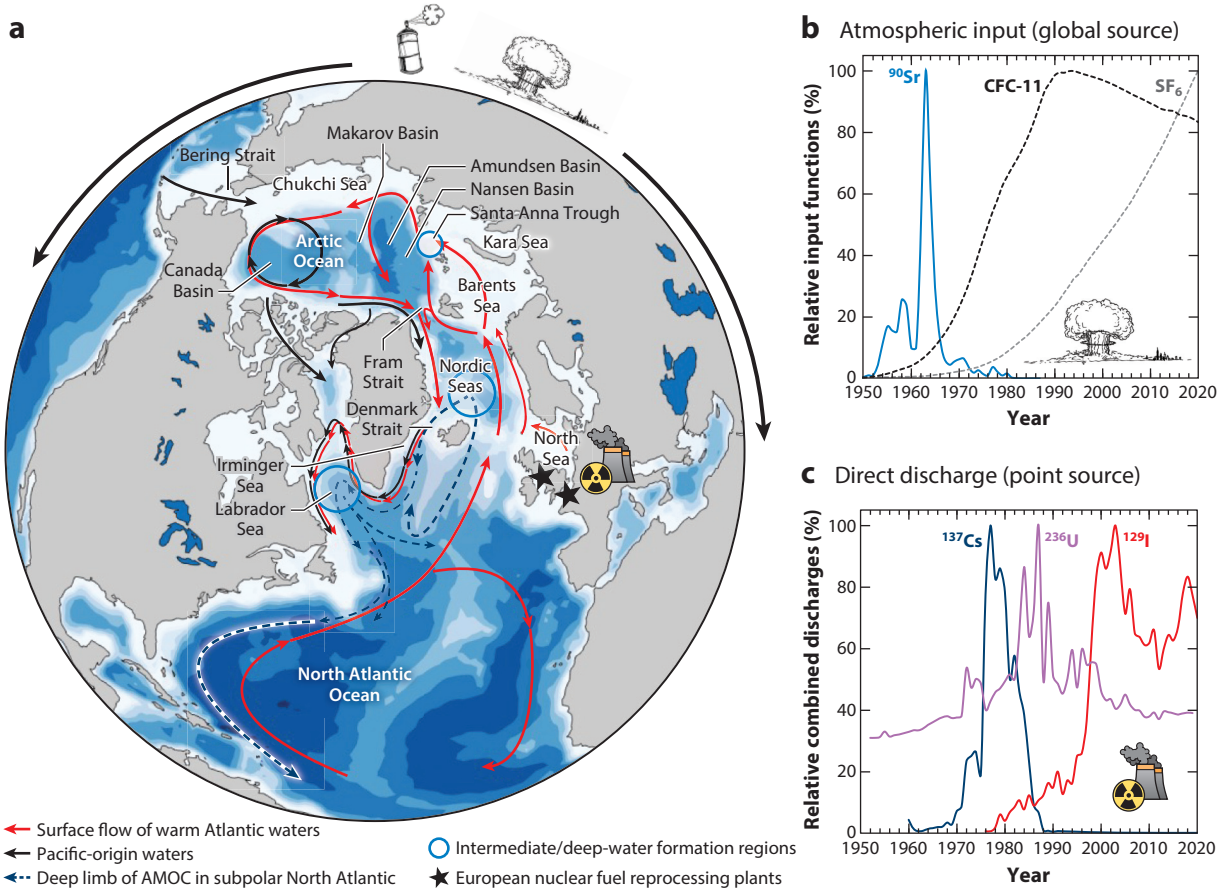

Figure 1

(*a*) Schematic map representing features of ocean circulation in the Arctic and subpolar North Atlantic Oceans. Red arrows represent the surface flow of warm AW entering the Arctic Ocean, where modified AW occupies depths up to 1,500 m; black arrows represent Pacific-origin waters; and blue arrows represent the deep limb of the AMOC in the subpolar North Atlantic. Blue circles represent the formation regions for intermediate- and deep-water masses that constitute the northern loop of the AMOC. Stars represent the two European nuclear fuel reprocessing plants, Sellafield and La Hague. (*b*) Relative input functions of the atmospheric transient tracers ^{90}Sr, CFC-11, and SF_6. (*c*) Relative combined discharges of ^{137}Cs, ^{236}U, and ^{129}I from the two European nuclear fuel reprocessing plants. Abbreviations: AMOC, Atlantic Meridional Overturning Circulation; AW, Atlantic Water; CFC, chlorofluorocarbon; SF_6, sulfur hexafluoride.

the AMOC is still a matter of debate (Boers 2021, Caesar et al. 2021, Le Bras et al. 2021, Lobelle et al. 2020). However, changes in the rates of deep-water formation have direct consequences for the ventilation of the deep ocean, the ocean's potential to store anthropogenic carbon (Sabine & Tanhua 2010), and the strength of the AMOC and its associated heat transport (Srokosz & Bryden 2015), and methods are required to evaluate and monitor these changes.

Radionuclides as Oceanographic Transient Tracers

Transient tracers are an effective and versatile tool for addressing issues in ocean circulation associated with climate change impacts in the Arctic and North Atlantic Oceans. A transient tracer is a

generally unreactive, soluble substance that is transported conservatively (i.e., is highly soluble in seawater, thus being distributed by physical processes related to ocean mixing and diffusion) and has been introduced to the ocean with an input function that is conducive to the illumination of kinetic rate information associated with circulation and mixing (Jenkins & Smethie 1996, Stöven et al. 2015). These tracers can be of natural or artificial nature and either globally dispersed or released from point sources (**Figure 1*b*,*c***), but most importantly, the source function (either as a long-term or pulsed release) must be well constrained. Once the transient tracers enter the marine environment, their utility depends on their effectiveness in labeling the progress of specific ocean processes on useful timescales, which in turn depends on their biological, chemical, and physical characteristics (Jenkins & Smethie 1996).

Some of the earliest substances used as time tracers in the ocean were the cosmogenically derived isotopes ^{14}C and ^{39}Ar. These elements are transferred into the ocean at the air–sea interface, and once isolated from the atmosphere, their water column concentrations are diminished by dilution and radioactive decay at a known rate, with this last process simulating a clock (Broecker & Peng 1982, Matsumoto 2007, Schlitzer 1986, Stuiver 1980). A major development in tracer oceanography occurred with the atmospheric dispersion of anthropogenic substances: weapon-test-derived radioactive tracers (^{3}H, ^{90}Sr, ^{137}Cs, etc.; **Figure 1*b*** includes only ^{90}Sr) and synthetic compounds, including chlorofluorocarbons (CFCs) and sulfur hexafluoride (SF_6), which were emitted into the atmosphere as nuclear and industrial by-products, respectively (Fine 2011, Livingston & Povinec 2002). The main difference between natural and anthropogenic tracers is that the former are generally produced at an approximately constant rate and rely on their precisely known decay constants and environmentally produced disruption of their decay chains to provide process information, while the latter imprints the experimental domain (e.g., sea surface, sediment, or organism) with a measurable time-dependent signature, also known as the input function. In the former case, the clock is usually the radionuclide decay rate; in the latter, the kinetic information is provided by the timing of the historical releases. The anthropogenic tracers are usually applied to processes occurring on timescales of approximately 100 years, corresponding to active human intervention in the environment, while the natural tracers have applications to processes extending over a wide range of timescales, ranging from modern to geological time (Stöven et al. 2015).

Artificial radionuclides have also been introduced into the marine environment from point sources as a result of controlled releases from the two European nuclear fuel reprocessing plants of Sellafield (formerly known as Windscale) in the United Kingdom and La Hague in France (**Figure 1*a***). These two facilities have been imprinting the North Sea with a unique set of artificial radionuclides since the 1960s (Kershaw & Baxter 1995; Kershaw et al. 1999; Smith et al. 1990, 1998, 1999). The radionuclide discharges (**Figure 1*c***) can be converted into input functions for the North Sea using empirically determined transfer factors that convert the discharges (kg/year) into a marine input function (atoms/L) (Edmonds et al. 2001, Smith et al. 2005) or using the output of a simple box model (Christl et al. 2015). The reprocessing plant tracers address similar timescales as anthropogenic gas tracers, but since they are discharged laterally into the ocean from point sources rather than vertically over broad areas by air–sea exchange, they have much greater geographical specificity and target specific bodies of water. For example, the release of reprocessing radionuclides into the North Sea permits their application as tracers in downstream marine systems, including the Nordic Seas, the Arctic Ocean, and eventually the deep North Atlantic and possibly more distant downstream regions of the AMOC (Edmonds et al. 1998; Karcher et al. 2004; Kershaw & Baxter 1995; Orre et al. 2010; Smith et al. 2005, 2016).

One of the first reprocessing plant–derived radionuclides used as an oceanographic tracer was ^{137}Cs (half-life of 30 years). Since the 1960s, ^{137}Cs has been a major component of discharges from

Annu. Rev. Mar. Sci. 2023.15:203-221. Downloaded from www.annualreviews.org
Access provided by ETH- Zurich on 07/24/23. See copyright for approved use.

the Sellafield nuclear fuel reprocessing plant (**Figure 1*c***). Studies of the seawater distribution of ^{137}Cs have provided remarkable insight into water circulation in the Irish and North Seas (Hetherington & Jefferies 1974; Jefferies et al. 1973, 1982) and in downstream regions such as the Nordic Seas (Dahlgaard et al. 1995, Kershaw & Baxter 1995, Kershaw et al. 1999, Livingston & Jenkins 1983, Livingston et al. 1982), the Denmark Strait (Edmonds et al. 2001, Livingston et al. 1985), and the central Arctic Ocean (Livingston et al. 1984; Smith & Ellis 1995; Smith et al. 1990, 1998, 1999). The ocean input function for the North Sea for ^{137}Cs was distinguished by a large peak in the late 1970s from Sellafield followed by a long decline over the subsequent years, interrupted very briefly by a pulsed input of ^{137}Cs from the 1986 Chernobyl accident in Ukraine (not shown in **Figure 1*c***). The simultaneous releases of another radiocesium isotope, ^{134}Cs, which has a half-life for radioactive decay of 2.1 years, permitted extremely accurate measurements of downstream transit times in the North and Nordic Seas (Livingston et al. 1982, Smith et al. 1990).

Annu. Rev. Mar. Sci. 2023.15:203-221. Downloaded from www.annualreviews.org
Access provided by ETH- Zurich on 07/24/23. See copyright for approved use.

^{129}I: A MAJOR ADVANCE IN TRACER OCEANOGRAPHY

The emergence of ^{129}I (half-life of 15.7 million years) as an oceanographic tracer in the 1980s coincided with both the decrease of ^{137}Cs releases from European nuclear fuel reprocessing plants and innovations in accelerator mass spectrometry techniques for the detection of ^{129}I in small seawater samples (<1 L) (Kilius et al. 1987, 1992). Although iodine is a biophilic element (i.e., it concentrates in seaweed), the observed residence time in the ocean ($\sim 10^5$ years) suggests that it behaves almost conservatively in the open ocean (Raisbeck et al. 1995). The uniqueness of ^{129}I as a marine tracer therefore rested with the geographic specificity and precise knowledge of its lateral inputs to the ocean, the accuracy of its measurement by accelerator mass spectrometry, and the simplicity of sampling owing to the absence of major environmental sources of ^{129}I contamination (Raisbeck & Yiou 1999, Raisbeck et al. 1995, Yiou et al. 1994). These characteristics provided a clear advantage over ^{137}Cs, a tracer that had other atmospheric and poorly constrained sources (i.e., weapons fallout and Chernobyl-derived contamination) and required larger sampling volumes of water (>20 L) due to the higher detection limits of the decay-counting technique mandatory for its measurement. The first studies proving the validity of ^{129}I as a new tool in oceanography demonstrated that the plume coming from the North Sea had been observable in 1976–1978 in Scottish and Norwegian coastal waters, corroborating predictions based on available release data and archived seaweed samples and confirming that the weapon-test contribution represented less than 1% of the reprocessing signal in the Norwegian Coastal Current (Alfimov et al. 2004b, Edmonds et al. 1998, Raisbeck et al. 1995). As discharges of ^{129}I increased after the 1990s, the tracer-labeled waters transported the signal through the Arctic Ocean and deep North Atlantic, imprinting the various ocean pathways with a detailed concentration discharge history that marked its flow on this long oceanic passage (Karcher et al. 2012; Orre 2008; Smith et al. 2011, 2016, 2021).

Pathways of Atlantic-Sourced Waters in the Arctic Ocean

Circulation pathways in the central Arctic Ocean are delineated in **Figure 2** using a large ^{129}I data set collected over the last decade. This quasi-synoptic three-dimensional view (**Figure 2*a***) of the ^{129}I distribution in the Arctic Ocean includes data from five expeditions that took place over the years 2012–2016 within the GEOTRACES program (GN01 and GN04 in 2015 in the central Arctic Ocean and GN05 in 2016 in Fram Strait), the Joint Ocean Ice Study cruise in 2015, and the Switchyard program in 2012 (Casacuberta et al. 2016, 2018; Smith et al. 2021; Wefing et al. 2019). As shown in **Figure 2*a***, the highest concentrations of ^{129}I were over the Barents Sea shelf, where a large proportion of the tracer signal from the European reprocessing plants is transported from the North Sea (Casacuberta et al. 2018). The high-^{129}I surface signal circulates cyclonically

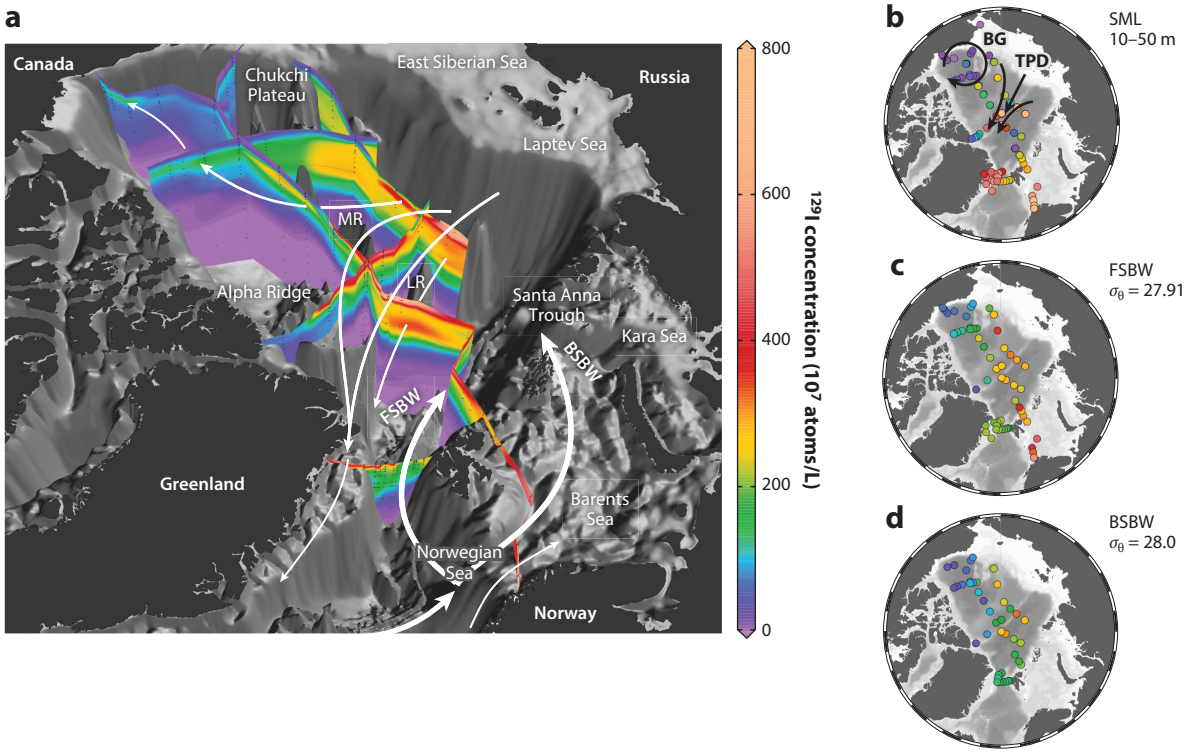

Figure 2

(*a*) Quasi-synoptic distribution of ^{129}I in the Arctic Ocean and Fram Strait during the period 2012–2016. Colors represent ^{129}I concentrations; white arrows emphasize the AW circulation. **Supplemental Video 1** provides a rotating view. (*b–d*) The same data on iso-surfaces of the SML (panel *b*), core FSBW ($\sigma_\theta = 27.91$) (panel *c*), and core BSBW ($\sigma_\theta = 28.00$) (panel *d*). Abbreviations: AW, Atlantic Water; BG, Beaufort Gyre; BSBW, Barents Sea Branch Water; FSBW, Fram Strait Branch Water; LR, Lomonosov Ridge; MR, Mendeleyev Ridge; SML, surface mixed layer; TPD, Transpolar Drift. Panel *a* provided by Reiner Schlitzer (Alfred Wegener Institute, Germany); data compiled from Casacuberta et al. (2016, 2018), Smith et al. (2021), and Wefing et al. (2019).

Annu. Rev. Mar. Sci. 2023.15:203-221. Downloaded from www.annualreviews.org
Access provided by ETH- Zurich on 07/24/23. See copyright for approved use.

Supplemental Material >

over the slopes and shelves of the Barents, Kara, and Laptev Seas, and upon encountering the Lomonosov Ridge and Mendeleyev Ridge, the signal is redirected back toward Fram Strait in association with the Transpolar Drift on the northern edge of the Beaufort Gyre. In contrast to the high concentrations of ^{129}I in the surface waters of Atlantic origin in the Eurasian Basin, levels of ^{129}I in the surface waters of Pacific origin in the Amerasian (Canada) Basin are very low (**Figure 2*b***). Since there is no significant ^{129}I reprocessing signal in the Pacific Ocean, PW entering the Arctic Ocean through the Bering Strait is labeled only by low levels of fallout ^{129}I, resulting in a clear boundary delineation between high-^{129}I AW and low-^{129}I PW.

Intermediate waters (200–1,000 m) of the Arctic Ocean are supplied by both the West Spitzbergen Current flowing through Fram Strait, termed Fram Strait Branch Water, and water flowing through the Barents Sea, termed Barents Sea Branch Water (**Figure 2*c*,*d***). These branches (characterized by different density levels) merge and partially mix in the Eurasian Basin near the mouth of the Santa Anna Trough and are responsible for most of the transport of heat to central Arctic Intermediate Water (Rudels 2009, Rudels et al. 2012). This combined water mass assembly extending over the depth range of 200–800 m circulates cyclonically through the Eurasian and Makarov Basins (**Figure 2*a*,*c*,*d***) while it undergoes bathymetric steering by the ridge systems generating

return flows toward Fram Strait. A component of intermediate water labeled by ^{129}I flows across the Lomonosov Ridge and through the region north of the Chukchi Plateau as it ventilates the interior of the Canada Basin (**Figure 2*a***). The lowest ^{129}I levels measured in intermediate waters of Atlantic origin are found in the northern Canada Basin near the Alpha Ridge, indicating that water mass ages in this region probably exceed 40 years (Smith et al. 2021). The deep waters below 2,000 m contain low ^{129}I levels ($<1 \times 10^7$ atoms/L; **Figure 2*a***) and have water residence times on the order of hundreds of years (Macdonald & Carmack 1991).

Changes in Arctic Ocean Circulation

In addition to delineating present circulation patterns, nuclear fuel reprocessing plant tracers such as ^{129}I can be used to reveal historical shifts in Arctic circulation associated with changes in climate indices. For example, the 2015 GEOTRACES cruise occupied stations that had previously been occupied during the Arctic Ocean Section cruise in 1994 (Carmack et al. 1997, Swift et al. 1997) (**Figure 3**). Prior to the 2015 cruise, large changes in the oceanic circulation pattern had been initiated in association with an abrupt increase in the Arctic Oscillation index in 1989 (NCEI 2022) and a coincident switch of the oceanic circulation regime in the Canada Basin (Proshutinsky et al. 2015) from anticyclonic (1985–1988) to cyclonic (1989–1996). During this period, the size of the Beaufort Gyre (**Figure 3*a***) was reduced and the Siberian river runoff was diverted eastward from its previous direct pathway into the Transpolar Drift (Steele & Boyd 1998). In addition, the boundary between Atlantic-derived surface waters (^{129}I levels $> 30 \times 10^7$ atoms/L in 1994) and Pacific-derived surface waters contaminated solely by fallout background ($^{129}\text{I} \cong 1\text{–}2 \times 10^7$ atoms/L) had shifted eastward from its position over the Lomonosov Ridge in the 1980s and had become aligned with the Mendeleyev Ridge (**Figure 3*b***). Below the halocline in the AW layer, anomalously warm AW entered the Makarov Basin along the Siberian slope (Carmack et al. 1997), providing a temperature anomaly that was subsequently traced throughout the Arctic Ocean (McLaughlin et al. 2009). This was accompanied by a strong AW boundary current flow over the continental slope of the Chukchi Sea delineated by elevated ^{129}I levels ($>50 \times 10^7$ atoms/L) over the 200–500-m depth range in the southern Makarov Basin (**Figure 3*b***). Under these mid-1990s cyclonic conditions, the dominant return flow of high-^{129}I ($>30 \times 10^7$ atoms/L) Atlantic surface water toward Fram Strait occurred over the flanks of both the Mendeleyev and Lomonosov Ridges (**Figure 3*b***).

Transport of ^{129}I through the Arctic Ocean has been simulated using a regional, coupled sea ice–ocean model termed the North Atlantic–Arctic Ocean–Sea Ice Model (NAOSIM) for the period from 1970 to 2015 (Karcher et al. 2012, Köberle & Gerdes 2003, Smith et al. 2021). **Figure 3*c*** shows the NAOSIM simulation of ^{129}I levels in surface waters in 1995, where the location of the front between AW and PW and the measured concentrations of ^{129}I that characterize this front are accurately simulated by the model. The front outlines the position of the Transpolar Drift that extended from the Chukchi Sea across the North Pole to Fram Strait in 1995, approximately following the 0°–180° axis of longitude.

The Arctic Oscillation reverted to an anticyclonic (negative) circulation regime in the early 2000s, and the main pathway for the flow of high-^{129}I surface water of Atlantic origin toward Fram Strait returned to the flank of the Lomonosov Ridge (**Figure 3*d***), where it was delineated by ^{129}I levels exceeding 800×10^7 atoms/L by 2015 (**Figure 3*e***). Note that in **Figure 3*e***, the ^{129}I concentration scale has been adjusted upward by an order of magnitude; this change is designed to account for the large ^{129}I spike that entered the Arctic Ocean in the mid-1990s and is intended to normalize tracer concentrations and make different annual ^{129}I section panels (**Figure 3*b*,*d***) comparable. It is clear that the 2015 ^{129}I results in the southern Makarov Basin

Annu. Rev. Mar. Sci. 2023.15:203-221. Downloaded from www.annualreviews.org
Access provided by ETH- Zurich on 07/24/23. See copyright for approved use.

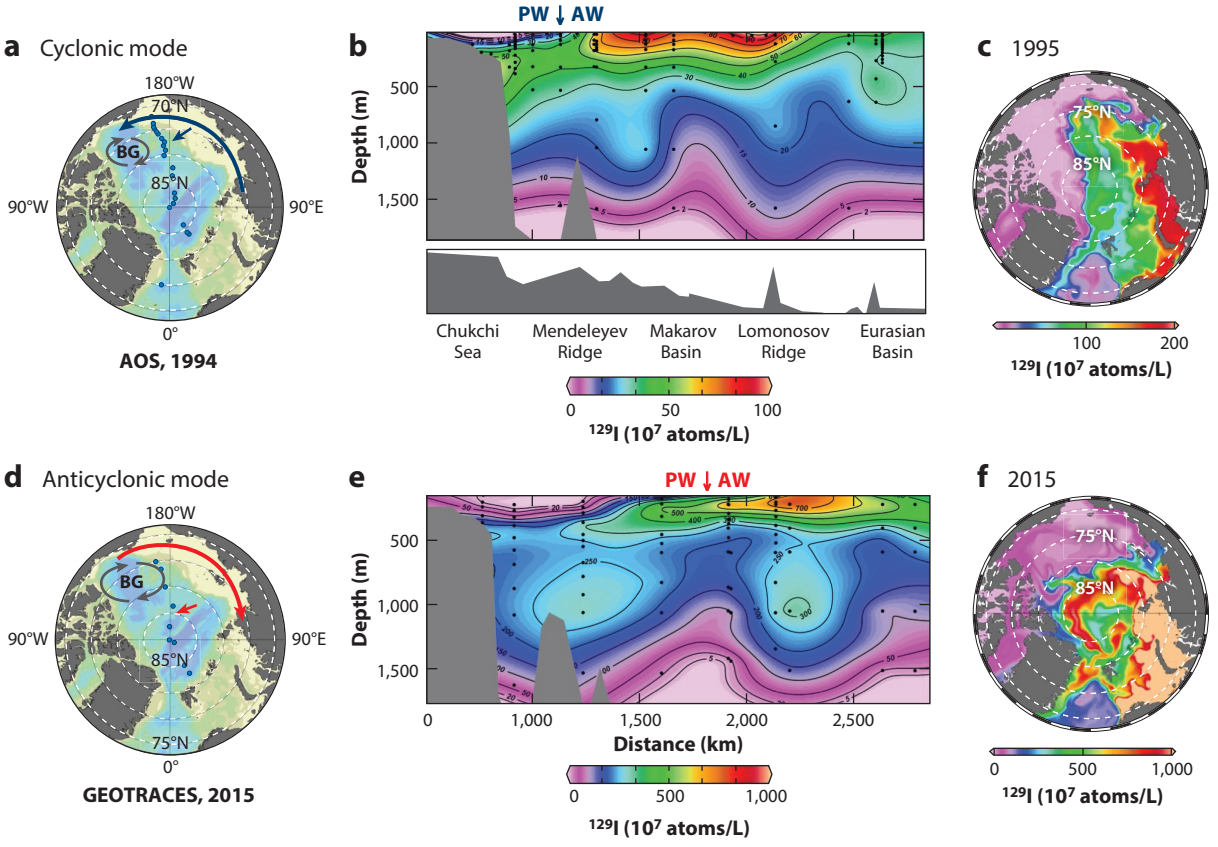

Figure 3

(*a*) AOS cruise track in 1994 (*blue dots*), when the Arctic Oscillation was strongly positive and the circulation was in a cyclonic mode (*curved blue arrow*). The straight arrow shows the location of the AW–PW interface indicated in panel *b*. (*b*) ^{129}I sections measured across the Makarov and Eurasian Basins during the same cruise, when the AW–PW interface defined by the ^{129}I front (*arrow* and *sections*, respectively) was positioned over the Mendeleyev Ridge. (*c*) NAOSIM simulation of the ^{129}I signal distribution in 1995 (Karcher et al. 2012). (*d*) GEOTRACES cruise in 2015 at the same stations occupied by the AOS cruise in 1994 (*blue dots*). The curved red arrow shows the circulation's anticyclonic mode, and the straight red arrow shows the location of the AW–PW interface indicated in panel *e*. (*e*) ^{129}I section measured in 2015, when the circulation had reverted to an anticyclonic mode and the AW–PW interface had returned to a position near the Lomonosov Ridge. (*f*) NAOSIM simulation of ^{129}I in the SML in 2015 (Smith et al. 2021), showing the new rotational alignment of the PW–AW interface with the Lomonosov Ridge. The ^{129}I input function (**Figure 1*c***) for intermediate water in the Arctic Ocean shows the arrival of a large ^{129}I spike in the late 1990s, resulting in a factor-of-10 increase in Arctic ^{129}I levels between 1994 and 2015. Note that the ^{129}I concentration scales have been increased for 2015 relative to those for 1994 to better compare the ^{129}I spatial distributions for the two different sampling periods. Abbreviations: AOS, Arctic Ocean Section; AW, Atlantic Water; BG, Beaufort Gyre; NAOSIM, North Atlantic–Arctic Ocean–Sea Ice Model; PW, Pacific Water; SML, surface mixed layer.

(**Figure 3*e***) show little evidence of a locally elevated ^{129}I signal in the upper intermediate water (≅400 m) near the continental margin, as was observed in 1994 (**Figure 3*b***), indicating that the AW boundary current had significantly weakened since the mid-1990s. In addition, the interface between high-^{129}I Atlantic-derived surface water and low-^{129}I Pacific-derived surface water had retreated to the Makarov Basin, as is also consistent with the NAOSIM simulation (**Figure 3*f***). These changes, which are present in both observations and models (Karcher et al. 2012), are driven by factors such as the shift from cyclonic to anticyclonic circulation

Annu. Rev. Mar. Sci. 2023.15:203-221. Downloaded from www.annualreviews.org
Access provided by ETH- Zurich on 07/24/23. See copyright for approved use.

regimes between the 1990s and 2000s, an accompanying acceleration and deepening of the Beaufort Gyre, and an increased volume of low-salinity waters in the Canada and Makarov Basins (Morison et al. 2012, Proshutinsky et al. 2009, Rabe et al. 2014). In particular, a comparison of NAOSIM results between 1995 and 2015 (**Figure 3*c*,*f***) shows that the AW–PW interface delineated by ^{129}I in the SML underwent an almost 90° rotation as a result of the shift of circulation regime (Smith et al. 2021), highlighting the utility of ^{129}I in tracking circulation changes associated with climate indices and the effectiveness of models in anticipating and confirming these changes.

^{129}I: TRACKING TRANSPORT BETWEEN OCEAN BASINS

One of the strengths of ^{129}I as an ocean tracer is its capacity of tracking transport between the different ocean basins as the plume of ^{129}I releases is transported downstream from its source region. Tracer-labeled waters exiting the North Sea imprint the AW with a signature that has changed over time, reflecting the historical releases of ^{129}I from the combination of Sellafield and La Hague (**Figure 1*c***). These waters can either enter the Arctic Ocean and ultimately outflow to the subpolar North Atlantic via Fram Strait or directly recirculate to the Nordic Seas without entering the Arctic Ocean. The ^{129}I tracer plume generated by the two reprocessing plants has been observed both within the Arctic Ocean (Alfimov et al. 2004b, Casacuberta et al. 2018, Smith et al. 2011) and in the subpolar and deep North Atlantic (Alfimov et al. 2013, Castrillejo et al. 2018, Edmonds et al. 1998, Santschi et al. 1996, Smith et al. 2005).

Figure 4 shows a compilation of time series measurements of ^{129}I for geographical locations at the North Pole and in the Labrador Sea and deep North Atlantic. The ^{129}I input function defined for the eastern Norwegian Sea at the entrance to the Arctic Ocean (**Figure 4*a***) is distinguished by the 1990s sharp increase in ^{129}I concentrations (**Figure 4*b***). At the North Pole (**Figure 4*b*,*c***), ^{129}I concentrations in the Atlantic layer (Arctic Intermediate Water) increased from 20×10^7 atoms/L in 1994 to almost 300×10^7 atoms/L in 2015 (**Figure 4*c***) in response to the 1990s increase in the input function (Alfimov et al. 2004b, Casacuberta et al. 2018, Smith et al. 2011). The ^{129}I time series is stretched in time compared with the input function owing to mixing. Tracer-labeled Arctic Intermediate Water exited the Arctic Ocean through Fram Strait (Alfimov et al. 2004a,b; Wefing et al. 2019); flowed southward through Denmark Strait with cold, dense East Greenland Current water (Alfimov et al. 2013, Edmonds et al. 2001); and descended 3,000 m to the bottom of the Irminger and Labrador Seas with Denmark Strait Overflow Water (Castrillejo et al. 2018, Smith et al. 2005). The ^{129}I time series in Denmark Strait Overflow Water in the Labrador Sea (**Figures 4*b***) exhibits an ^{129}I increase from 10×10^7 atoms/L in 1993 to close to 100×10^7 atoms/L in 2015 (**Figure 4*d***). This time series has a stepwise shape distinguished by significant increases in 1999–2001 and 2010–2012 (**Figure 4*b***) that were neither observed in the North Pole time series nor represented in the original input function for the Norwegian Sea. The first tracer concentration step in 1999–2001 represents ^{129}I-labeled AW from the Norwegian Sea that has bypassed the Arctic Ocean via recirculation in Fram Strait followed by southward flow through Denmark Strait and descent into the deep Labrador Sea on timescales of approximately 3–5 years (Smith et al. 2005, 2016). The second tracer step represents the increase of ^{129}I associated with tracer-labeled AW following the entire circulation pathway through the central Arctic Ocean (Castrillejo et al. 2018), which adds approximately 8 years to its passage, followed by its exit through Fram Strait, where it merges with the initial short-circuiting branch of AW.

Following its flow across the bottom of the Labrador Sea, Denmark Strait Overflow Water joins the Deep Western Boundary Current, which flows southward along the flank of the North American continental slope from subpolar to subtropical domains. A time series of ^{129}I

Annu. Rev. Mar. Sci. 2023.15:203-221. Downloaded from www.annualreviews.org
Access provided by ETH- Zurich on 07/24/23. See copyright for approved use.

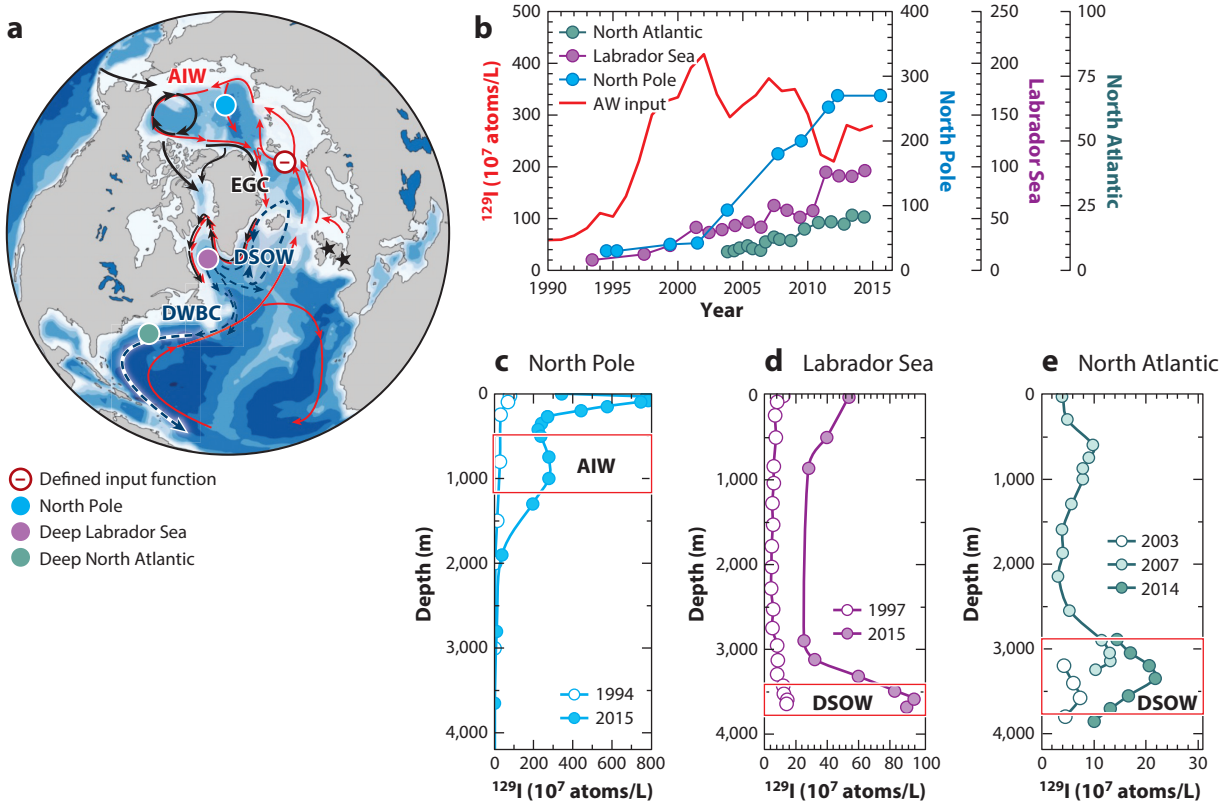

Figure 4

(*a*) Geographical locations where the input function is defined (*open red circle*) and time series have been performed since the 1990s (the North Pole, *blue dot*; the deep Labrador Sea, *purple dot*; and the deep North Atlantic on Line W, *teal dot*). (*b*) Input function (*red*) and temporal evolution of ^{129}I concentrations at the North Pole (*blue*), in the deep Labrador Sea (*purple*), and in the deep North Atlantic (*teal*). (*c–e*) The earliest (*open circles*) and latest (*filled circles*) profiles measured at the North Pole (panel *c*), in the Labrador Sea (panel *d*), and in the North Atlantic (panel *e*). Note that panel *e* also shows a full water profile for the year 2007 (in 2003 and 2014, only deep samples were taken). Red outlined areas identify AIW at the North Pole and DSOW in the deep Labrador Sea and on Line W (Cape Cod to Bermuda) in the North Atlantic. ^{129}I values in panel *b* correspond to mean annual values measured for water masses denoted in panels *c–e*. Abbreviations: AIW, Arctic Intermediate Water; AW, Atlantic Water; DSOW, Denmark Strait Overflow Water; DWBC, Deep Western Boundary Current; EGC, East Greenland Current. Data compiled from Alfimov et al. (2004a), Casacuberta et al. (2016, 2018), and Smith et al. (2005, 2011, 2016).

was measured on Line W in the North Atlantic (**Figure 4*b*,*e***), a heavily instrumented section established from Cape Cod to Bermuda that was operative from 2004 to 2014 (Smith et al. 2016, Toole et al. 2017). ^{129}I levels in the Denmark Strait Overflow Water component of the Deep Western Boundary Current in the 3,200–4,000-m depth range increased from approximately 6×10^7 atoms/L to 22×10^7 atoms/L over the 10-year experiment (**Figure 4*e***) as the ^{129}I spike observed upstream in the deep Labrador Sea passed across Line W in the deep North Atlantic. A boundary current model applied to the interpretation of the time series tracer data revealed that transport from the Labrador Sea to Line W occurs on a timescale of 5–6 years and has a mean flow velocity of 2.7 cm/s, while mixing between the core and interior of the boundary current occurs with a time constant of 2.6 years (Smith et al. 2016). Similarly elevated ^{129}I levels over the southern Bermuda slope revealed interior pathways for flow from the Labrador Sea that would also ventilate abyssal waters of the deep North Atlantic (Castrillejo et al. 2022).

Annu. Rev. Mar. Sci. 2023.15:203-221. Downloaded from www.annualreviews.org
Access provided by ETH- Zurich on 07/24/23. See copyright for approved use.

During the long passage from the surface waters of the North Sea to depths of 3,800 m on Line W in the deep North Atlantic, the ^{129}I signal underwent significant dilution as a result of mixing with tracer-free AW, and the slope of the initially steep tracer input spike gradually decreased in comparison with the North Pole and Labrador Sea time series. However, the ^{129}I input spike itself is quite clearly resolved even after a 14,000-km transit through the Arctic and North Atlantic Oceans, indicating that reprocessing tracers may be similarly effective in connecting oceans and delineating flow pathways along even more distant intervals of the AMOC.

COMBINING REPROCESSING TRACERS

Tracer applications using multiple independent tracers can provide considerable insight into flow features because this approach permits control over several operational variables, such as advective velocity and dilution by tracer-free water. This approach has long been adopted in the analysis of gas tracer combinations such as tritium–helium and CFC-11–SF_6, which have been critical in shaping our understanding of ventilation and transport in the ocean (Fine 2011, Smethie et al. 2000, Stöven et al. 2015). In a similar fashion, Smith and coworkers made use of the well-constrained input functions of CFC-11, ^{129}I, and ^{137}Cs to determine circulation times and mixing regimes for AW transport from the North Sea (60°N) to different polar (Smith et al. 1998, 1999, 2011), subpolar (Smith et al. 2005), and subtropical (Smith et al. 2016) regions. The combination of ^{129}I with both CFC-11 and ^{137}Cs highlighted the strength of using tracers with different input histories, because this approach permits a unique solution to the determination of tracer ages, defined as the elapsed time since an interior concentration was equivalent to that of the input function.

Tracer Ages for the Arctic Surface Mixed Layer

Tracer ages for SML water (depth ≤60 m) estimated using the tracer pair ^{129}I–^{137}Cs are summarized in **Figure 5*a*,*b***, referenced with respect to the transit time from the North Sea and corrected for background fallout for both ^{129}I and ^{137}Cs (Smith et al. 2011). This figure compiles data from a wide range of sampling platforms for 1994–2002 (**Figure 5*a***). The flow of Atlantic surface water eastward through the Russian marginal seas during the 1990s was delineated by the geographic distribution of tracer ages: 0.5–1 year for the western Barents Sea, 3 years for the eastern Barents Sea, 3–6 years for the Kara Sea, 6–7 years for the Laptev Sea, and 7 years for the East Siberian Sea (**Figure 5*a*,*b***). These measurements were conducted at a time (1993–1995) when the Arctic Oscillation was in a strongly positive phase and Atlantic surface water had spread eastward along the Russian continental shelf into the East Siberian Sea and eastern Makarov Basin. As a result, the tracer ages in the southern Makarov Basin for Atlantic surface water were 6–8 years, even less than those at the North Pole (9–12 years). The interface between Atlantic-origin and Pacific-origin SML water was aligned with the Mendeleyev Ridge during the mid-1990s and was delineated by a sharp ^{129}I gradient characterized by concentrations of 100×10^7 atoms/L in the former and 5×10^7 atoms/L in the latter. These circumstances permitted estimates of tracer ages for Atlantic surface water in the eastern Makarov Basin during the 1990s, even though no such estimates can be made for Pacific surface water, which lacks a suitable ^{129}I tracer signal.

Although the simultaneous use of ^{129}I and ^{137}Cs had the advantage of having the same source region in the North Sea and different input functions (Smith et al. 1998), the increasingly low concentrations of ^{137}Cs associated with discharges from the Sellafield and La Hague nuclear fuel reprocessing plants were becoming difficult to distinguish from delayed inputs of Chernobyl-derived ^{137}Cs that had been deposited in various Baltic Sea catchment basins and were now undergoing remobilization and transport into the North Sea (Smith et al. 2011). This factor (together with

Annu. Rev. Mar. Sci. 2023.15:203-221. Downloaded from www.annualreviews.org
Access provided by ETH- Zurich on 07/24/23. See copyright for approved use.

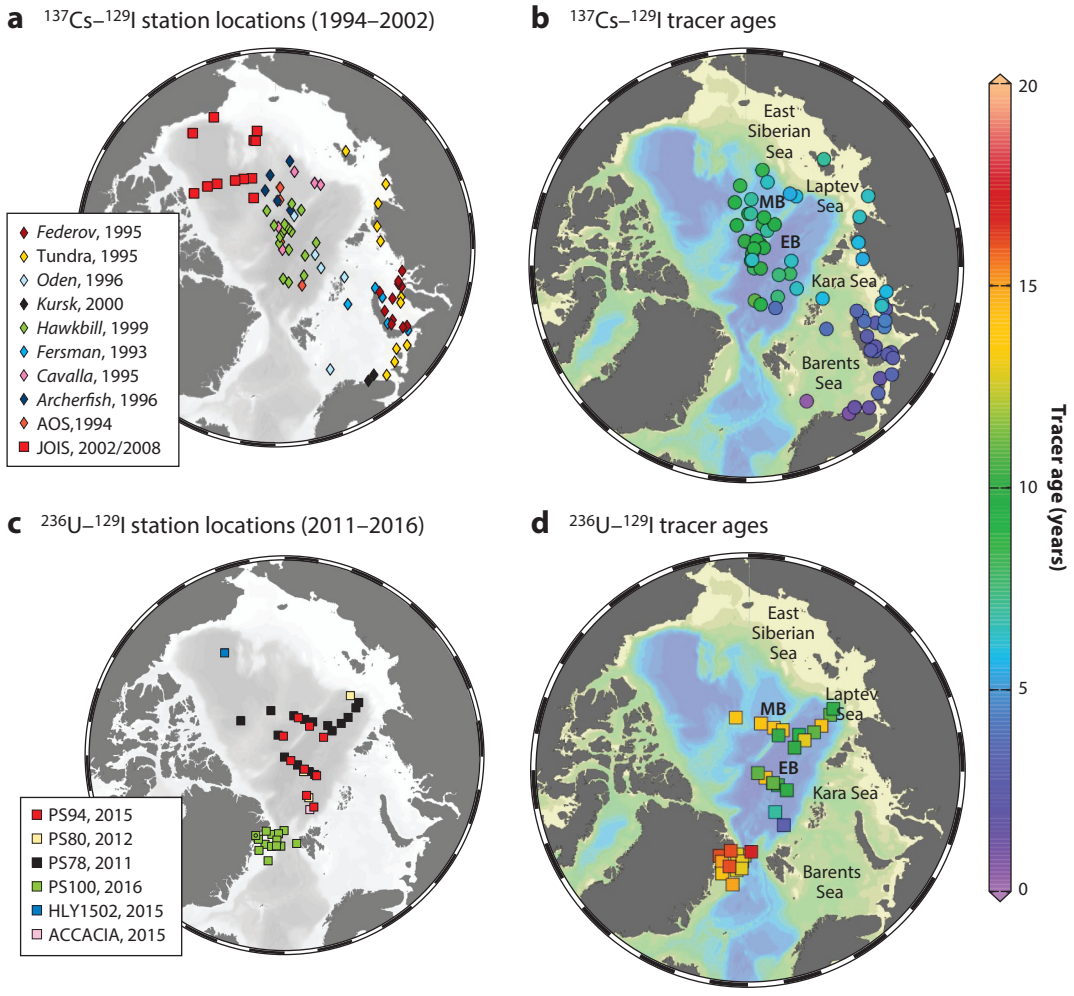

Figure 5

(*a*) Station locations for tracer age measurements (and TTD; see **Figure 6**) using the ^{129}I–^{137}Cs tracer pair. (*b*) Values of tracer ages in SML water determined using the ^{129}I–^{137}Cs tracer pair. (*c*) Station locations for tracer age measurements (and TTD; see **Figure 6**) using the ^{129}I–^{236}U tracer pair. (*d*) Values of tracer ages in SML water determined using the ^{129}I–^{236}U tracer pair. Note that some stations represented in panels *a* and *c* are used only to show TTD results in **Figure 6**. Abbreviations: ACCACIA, Aerosol–Cloud Coupling and Climate Interactions in the Arctic; AOS, Arctic Ocean Section; EB, Eurasian Basin; JOIS, Joint Ocean Ice Study; MB, Makarov Basin; SML, surface mixed layer; TTD, transit time distribution.

the larger sampling volumes of water required for its measurement) encouraged the search for new tracers. Similarly to the origination of ^{129}I methodologies in the 1980s, ongoing developments in accelerator mass spectrometry led to improved techniques for the measurement of ^{236}U (Steier et al. 2008), another long-lived radionuclide (half-life of 23 million years) that is discharged by the European nuclear fuel reprocessing plants (Christl et al. 2012, 2013, 2017). This technical advance, combined with modeling developments in the reconstruction of the historical inputs of ^{236}U from reprocessing plants (Christl et al. 2015) and validation using a novel shell archive (Castrillejo et al. 2020), facilitated the application of ^{236}U as a water mass tracer in the Arctic and Atlantic Oceans (Casacuberta et al. 2014, 2016). The combination of ^{129}I and ^{236}U has become a

Annu. Rev. Mar. Sci. 2023.15:203-221. Downloaded from www.annualreviews.org
Access provided by ETH- Zurich on 07/24/23. See copyright for approved use.

useful tracer pair for determining circulation timescales and mixing parameters, similarly to the combination of ^{129}I and ^{137}Cs but with greater precision (Casacuberta et al. 2018, Wefing et al. 2021).

A comparison of tracer age distributions for ^{129}I–^{236}U (Wefing et al. 2021) with those for ^{129}I–^{137}Cs in SML water in the central Arctic Ocean is illustrated in **Figure 5*b*,*d***. Both sets of tracers give tracer ages on the order of 8–14 years in the Makarov and Eurasian Basins, but the ^{129}I–^{236}U ages tend to be approximately 3 years greater than those of the ^{129}I–^{137}Cs pair at the few locations where both were used. The latter tracer pair was measured primarily during the 1990s, when circulation was in a cyclonic mode, while the former was measured mainly in the mid-2010s, under anticyclonic conditions, so differences in the tracer ages may reflect faster flow of SML water through the central Arctic Ocean under the 1990s cyclonic circulation regime.

Transit Time Distributions

A major shortcoming of early ocean tracer studies is that they neglected mixing and generally assumed advective flow. However, mass transport in the Arctic Ocean is significantly influenced by multiple modes of mixing (e.g., eddy mixing and double diffusive processes), and tracer circulation models were required that incorporated mixing or recirculation within the flow field. Several authors (Waugh & Hall 2005, Waugh et al. 2003) have noted that there is no single, unique transit time that describes fluid flow in the ocean. Instead, the flow of water arriving at a specific location is more accurately characterized by a range of transit times termed the transit time distribution (TTD) (Beining & Roether 1996, Haine & Hall 2002). Tracers with different input functions weight the TTD in different ways and can provide different estimates of tracer ages for the same flow structure, but the TTD itself is an intrinsic property of the flow from a specified source region (Waugh et al. 2003). The TTD method is based on the supposition that the concentration, c, of a tracer at point r and time t is given by

$$c(r,t) = \int_0^\infty c_0(t-t')e^{-\lambda t'} G(r,t')\mathrm{d}t', \qquad 1.$$

where c_0 is the upstream tracer input function, λ is the decay constant for radioactive tracers, and $G(r,t')$ is the TTD. $G(t)$ is usually assumed to have the form of an inverse Gaussian function,

$$G(t) = \sqrt{\frac{\Gamma^3}{4\pi\Delta^2 t^3}} \exp\left[\frac{-\Gamma(t-\Gamma)^2}{4\Delta^2 t}\right], \qquad 2.$$

which can be uniquely defined by two independent parameters: Γ, which is the mean age, and Δ, which is related to the width of the TTD and therefore to the amount of mixing. A third useful metric is the maximum in the TTD at a value of t termed the mode age, t_{max}, which under certain conditions is related to the observed advection time for the flow of a volume element of water. A wide range of interior tracer concentrations, $c(r,t)$, in the ocean can be calculated using Equation 1 by varying the values of Γ and Δ (Equation 2). These results can then be compared with experimental data sets to determine the best fits to the theoretical results and thereby constrain the values of Γ and Δ associated with the data sets.

Smith et al. (2011) used the tracer pair ^{129}I–^{137}Cs to estimate values of Γ and Δ for intermediate waters (core Fram Strait Branch Water, $\sigma_\theta = 27.91$) in the Arctic Ocean. They found good agreement between values of tracer ages and Γ for SML water but comparatively higher values of tracer ages for intermediate waters. These results indicated that the assumption of advective transport was applicable only to surface-water transport, while mixing was a significant factor for intermediate (250–1,000-m depth) Atlantic-derived waters. Wefing et al. (2021) applied a TTD

Annu. Rev. Mar. Sci. 2023.15:203-221. Downloaded from www.annualreviews.org
Access provided by ETH- Zurich on 07/24/23. See copyright for approved use.

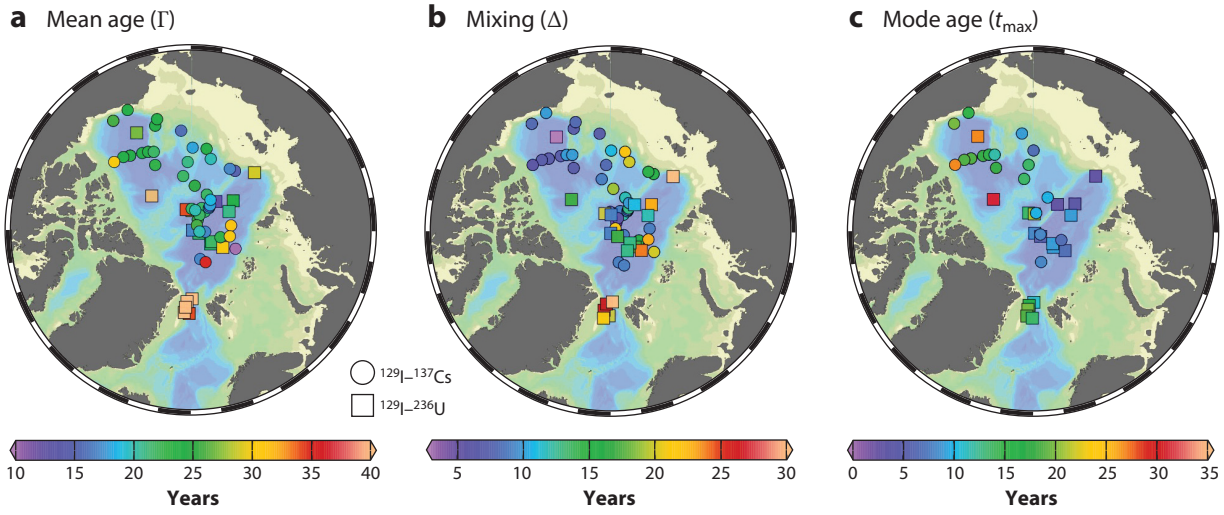

Figure 6

Results for TTD analyses of data from Atlantic Intermediate Water (200–500-m depth) for cruises and sampling years given in **Figure 5**. The data are for the tracer pairs ^{129}I–^{137}Cs (*circles*) and ^{129}I–^{236}U (*squares*), showing (*a*) mean ages, Γ; (*b*) mixing, Δ; and (*c*) mode ages, t_{max}. Abbreviation: TTD, transit time distribution. Data compiled from Smith et al. (2011) and Wefing et al. (2021).

model to studies of the new tracer pair ^{129}I–^{236}U; comparisons of their TTD results with those of Smith et al. (2011) are shown in **Figure 6**. The values of Γ, Δ, and t_{max} determined using the two different tracer pairs are in relatively good agreement even though the two studies occurred more than 10 years apart.

The mean ages, Γ, determined for core Fram Strait Branch Water using the two tracer pairs (**Figure 6*a***) generally increased across the central Arctic Ocean from the Makarov and Eurasian Basins into the Canada Basin. Values of Δ tend to be relatively constant across the central Arctic Ocean, with values in the 5–10-year range for measurements by both methods (**Figure 6*b***), indicating that transport across the Lomonosov Ridge into the Amerasian Basin has a stronger advective component than water recirculating within the Eurasian Basin. Apparently, most of the mixing defined by Δ in the central Arctic Ocean occurs upstream during AW transport through the Arctic shelf seas or over the respective continental slopes. Mode ages (**Figure 6*c***) are lower than mean ages, with values of 5–10 years in the Eurasian Basin increasing to values of approximately 15–25 years in the Canada Basin. Mode ages tend to be similar to transit times observed for the transport of hydrographic features such as warm temperature anomalies across the central Arctic Ocean (Karcher et al. 2003, McLaughlin et al. 2009).

Values of Γ, Δ, and t_{max} determined using reprocessing plant tracer pairs (i.e., ^{129}I–^{137}Cs and ^{129}I–^{236}U) have been compared with values estimated using a gas tracer pair (SF_6–CFC-11) (**Figure 7**). In general, results determined using the different methods are in reasonable agreement, except for two samples collected in the Nansen Basin in 2015, where the tracer pair ^{129}I–^{236}U seems to indicate greater mean ages (**Figure 7*a***), possibly associated with stronger mixing (Wefing et al. 2021) (**Figure 7*b***). Since mean ages tend to be more heavily weighted toward the higher values in the tail of the TTD, it may be that the mode age, which provides the best agreement among all tracer pairs (**Figure 7*c***), represents a more useful parameter to characterize flow velocities in the Arctic Ocean. However, this topic is still under debate, and additional multi-tracer studies are required.

Annu. Rev. Mar. Sci. 2023.15:203-221. Downloaded from www.annualreviews.org
Access provided by ETH- Zurich on 07/24/23. See copyright for approved use.

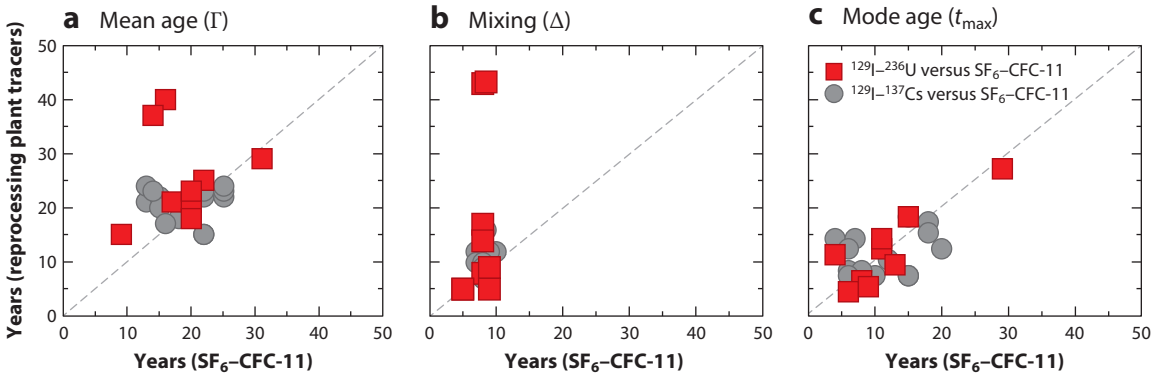

Figure 7

Comparisons of (*a*) mean age, Γ; (*b*) mixing, Δ; and (*c*) mode age, t_{max}, for the reprocessing plant tracer pairs ^{129}I–^{137}Cs and ^{129}I–^{236}U and the gas tracer pair SF_6–CFC-11. The comparisons of ^{129}I–^{236}U and SF_6–CFC-11 are from identical stations on PS94 and HLY1502 in 2015 (see **Figure 5**); the ^{129}I–^{137}Cs data are from pre-2002 cruises. Abbreviations: CFC, chlorofluorocarbon; SF_6, sulfur hexafluoride. Figure adapted from Smith et al. (2022).

CONCLUSIONS

Releases of radionuclides from the nuclear fuel reprocessing plants at Sellafield and La Hague have provided unique tracers for studies of water circulation in the local environment (the Irish Sea, English Channel, and North Sea) and larger-scale circulation processes of the North Atlantic and Arctic Oceans. The fact that they are released at regulated, industrial point sources makes them highly specific tracers with well-defined input functions. The most important reprocessing plant tracer through the 1980s and 1990s was ^{137}Cs, which was used to document the connectivity of European coastal waters to the central Arctic Ocean through its detection at early Arctic ice stations occupied in the 1980s in the Canada Basin and at the North Pole. However, recent advances in accelerator mass spectrometry techniques have been made in the measurement of ^{129}I and ^{236}U, which are long-lived radioactive tracers that are conservative in seawater and can be measured on small water samples (<500 mL and 3 L, respectively) practically anywhere in the Arctic and North Atlantic Oceans. ^{129}I has been applied to the delineation of water circulation patterns in the Arctic Ocean under the influence of changes in the Arctic Oscillation, from a cyclonic circulation in the 1990s, when it was in a strong positive mode, to an anticyclonic circulation in 2015, when it was in a mixed positive/negative mode. ^{129}I has also been used in the deep North Atlantic 14,000 km downstream from its point sources to determine flow and mixing rates for the Deep Western Boundary Current and for transport along interior flow pathways. One of the most significant recent developments in this field is the application of TTDs to the determination of mean ages, mode ages, and mixing parameters to more realistically characterize the ocean transport of ^{129}I and ^{236}U, complementing ventilation rates estimated from the gas tracers SF_6 and CFC. These two tracers experience little complication from other sources and hold great promise for elucidating circulation, deep-water formation, and ventilation processes in the North Atlantic, Nordic Seas, and Arctic Ocean in future years.

DISCLOSURE STATEMENT

The authors are not aware of any affiliations, memberships, funding, or financial holdings that might be perceived as affecting the objectivity of this review.

Annu. Rev. Mar. Sci. 2023.15:203-221. Downloaded from www.annualreviews.org
Access provided by ETH- Zurich on 07/24/23. See copyright for approved use.

ACKNOWLEDGMENTS

N.C. is currently funded by the European Research Council (ERC Consolidator grant GAP-101001451) and the Swiss National Science Foundation (PRIMA grant PR00P2_193091). Acknowledgments also go to the Laboratory of Ion Beam Physics (ETH Zürich) and the PhD students, postdocs, and technicians who helped generate some of the data that are summarized in this review. A special thanks goes to A.-M. Wefing and M. Castrillejo for their dedication, motivation, and fruitful discussions. We also thank Reiner Schlitzer (Alfred Wegener Institute, Germany) for the three-dimensional image shown in **Figure 2*a***. A final thanks goes to Ken Buesseler, who helped to considerably improve the text and figures.

LITERATURE CITED

Alfimov V, Aldahan A, Possnert G. 2004a. Tracing water masses with ^{129}I in the western Nordic Seas in early spring 2002. *Geophys. Res. Lett.* 31:L19305

Alfimov V, Aldahan A, Possnert G. 2013. Water masses and ^{129}I distribution in the Nordic Seas. *Nucl. Instrum. Methods Phys. Res. B* 294:542–46

Alfimov V, Aldahan A, Possnert G, Winsor P. 2004b. Anthropogenic iodine-129 in seawater along a transect from the Norwegian coastal current to the North Pole. *Mar. Pollut. Bull.* 49:1097–104

Beining P, Roether W. 1996. Temporal evolution of CFC 11 and CFC 12 concentrations in the ocean interior. *J. Geophys. Res. Oceans* 101:16455–64

Boers N. 2021. Observation-based early-warning signals for a collapse of the Atlantic Meridional Overturning Circulation. *Nat. Clim. Change* 11:680–88

Broecker WS, Peng T-H. 1982. *Tracers in the sea*. Rep., Lamont-Doherty Geol. Obs., Columbia Univ., Palisades, NY

Caesar L, McCarthy GD, Thornalley DJR, Cahill N, Rahmstorf S. 2021. Current Atlantic Meridional Overturning Circulation weakest in last millennium. *Nat. Geosci.* 14:118–20

Cao Y, Liang S, Chen X, He T, Wang D, Cheng X. 2017. Enhanced wintertime greenhouse effect reinforcing Arctic amplification and initial sea-ice melting. *Sci. Rep.* 7:8462

Carmack E, Polyakov I, Padman L, Fer I, Hunke E, et al. 2015. Toward quantifying the increasing role of oceanic heat in sea ice loss in the new Arctic. *Bull. Am. Meteorol. Soc.* 96:2079–105

Carmack EC, Aagaard K, Swift JH, MacDonald RW, McLaughlin FA, et al. 1997. Changes in temperature and tracer distributions within the Arctic Ocean: results from the 1994 Arctic Ocean Section. *Deep-Sea Res. II* 44:1487–502

Casacuberta N, Christl M, Lachner J, van der Loeff MR, Masque P, Synal HA. 2014. A first transect of ^{236}U in the North Atlantic Ocean. *Geochim. Cosmochim. Acta* 133:34–46

Casacuberta N, Christl M, Vockenhuber C, Wefing A-M, Wacker L, et al. 2018. Tracing the three Atlantic branches entering the Arctic Ocean with ^{129}I and ^{236}U. *J. Geophys. Res. Oceans* 123:6909–21

Casacuberta N, Masque P, Henderson G, van der Loeff MR, Bauch D, et al. 2016. First ^{236}U data from the Arctic Ocean and use of ^{236}U/^{238}U and ^{129}I/^{236}U as a new dual tracer. *Earth Planet. Sci. Lett.* 440:127–34

Castrillejo M, Casacuberta N, Christl M, Vockenhuber C, Synal HA, et al. 2018. Tracing water masses with ^{129}I and ^{236}U in the subpolar North Atlantic along the GEOTRACES GA01 section. *Biogeosciences* 15:5545–64

Castrillejo M, Casacuberta N, Vockenhuber C, Lherminier P. 2022. Rapidly increasing artificial iodine highlights pathways of Iceland-Scotland Overflow Water and Labrador Sea Water. *Front. Mar. Sci.* 9:897729

Castrillejo M, Witbaard R, Casacuberta N, Richardson CA, Dekker R, et al. 2020. Unravelling 5 decades of anthropogenic ^{236}U discharge from nuclear reprocessing plants. *Sci. Total Environ.* 717:137094

Christl M, Casacuberta N, Lachner J, Herrmann J, Synal H-A. 2017. Anthropogenic ^{236}U in the North Sea – a closer look into a source region. *Environ. Sci. Technol.* 51:12146–53

Christl M, Casacuberta N, Vockenhuber C, Elsässer C, Bailly du Bois P, et al. 2015. Reconstruction of the ^{236}U input function for the Northeast Atlantic Ocean: implications for ^{129}I/^{236}U and ^{236}U/^{238}U-based tracer ages. *J. Geophys. Res. Oceans* 120:7282–99

Annu. Rev. Mar. Sci. 2023.15:203-221. Downloaded from www.annualreviews.org
Access provided by ETH- Zurich on 07/24/23. See copyright for approved use.

Christl M, Lachner J, Vockenhuber C, Goroncy I, Herrmann J, Synal H-A. 2013. First data of uranium-236 in the North Sea. *Nucl. Instrum. Methods Phys. Res. B* 294:530–36
Christl M, Lachner J, Vockenhuber C, Lechtenfeld O, Stimac I, et al. 2012. A depth profile of uranium-236 in the Atlantic Ocean. *Geochim. Cosmochim. Acta* 77:98–107
Dahlgaard H, Chen Q, Herrmann J, Nies H, Ibbett RD, Kershaw PJ. 1995. On the background level of ^{99}Tc, ^{90}Sr and ^{137}Cs in the North Atlantic. *J. Mar. Syst.* 6:571–78
Edmonds HN, Smith JN, Livingston HD, Kilius LR, Edmond JM. 1998. ^{129}I in archived seawater samples. *Deep-Sea Res. I* 45:1111–25
Edmonds HN, Zhou ZQ, Raisbeck GM, Yiou F, Kilius LR, Edmond JM. 2001. Distribution and behavior of anthropogenic ^{129}I in water masses ventilating the North Atlantic Ocean. *J. Geophys. Res. Oceans* 106:6881–94
Fine RA. 2011. Observations of CFCs and SF_6 as ocean tracers. *Annu. Rev. Mar. Sci.* 3:173–95
Frajka-Williams E, Ansorge IJ, Baehr J, Bryden HL, Chidichimo MP, et al. 2019. Atlantic Meridional Overturning Circulation: observed transport and variability. *Front. Mar. Sci.* 6:260
Haine TWN, Hall TM. 2002. A generalized transport theory: water-mass composition and age. *J. Phys. Oceanogr.* 32:1932–46
Hetherington JA, Jefferies DF. 1974. The distribution of some fission product radionuclides in sea and estuarine sediments. *Neth. J. Sea Res.* 8:319–38
Jefferies DF, Preston A, Steele AK. 1973. Distribution of caesium-137 in British coastal waters. *Mar. Pollut. Bull.* 4:118–22
Jefferies DF, Steele AK, Preston A. 1982. Further studies on the distribution of ^{137}Cs in British coastal waters—I. Irish Sea. *Deep-Sea Res. A* 29:713–38
Jenkins WJ, Smethie WM Jr. 1996. Transient tracers track ocean climate signals. *Oceanus* 39(2):29–32
Jochumsen K, Köllner M, Quadfasel D, Dye S, Rudels B, Valdimarsson H. 2015. On the origin and propagation of Denmark Strait overflow water anomalies in the Irminger Basin. *J. Geophys. Res. Oceans* 120:1841–55
Karcher MJ, Gerdes R, Kauker F, Köberle C. 2003. Arctic warming: evolution and spreading of the 1990s warm event in the Nordic seas and the Arctic Ocean. *J. Geophys. Res. Oceans* 108:3034
Karcher MJ, Gerland S, Harms IH, Iosjpe M, Heldal HE, et al. 2004. The dispersion of ^{99}Tc in the Nordic Seas and the Arctic Ocean: a comparison of model results and observations. *J. Environ. Radioact.* 74:185–98
Karcher MJ, Smith JN, Kauker F, Gerdes R, Smethie WM Jr. 2012. Recent changes in Arctic Ocean circulation revealed by iodine-129 observations and modeling. *J. Geophys. Res. Oceans* 117:C08007
Kershaw PJ, Baxter A. 1995. The transfer of reprocessing wastes from north-west Europe to the Arctic. *Deep-Sea Res. II* 42:1413–48
Kershaw PJ, McCubbin D, Leonard KS. 1999. Continuing contamination of north Atlantic and Arctic waters by Sellafield radionuclides. *Sci. Total Environ.* 237–238:119–32
Khatiwala S, Tanhua T, Mikaloff Fletcher S, Gerber M, Doney SC, et al. 2013. Global ocean storage of anthropogenic carbon. *Biogeosciences* 10:2169–91
Kieke D, Yashayaev I. 2015. Studies of Labrador Sea Water formation and variability in the subpolar North Atlantic in the light of international partnership and collaboration. *Prog. Oceanogr.* 132:220–32
Kilius LR, Litherland AE, Rucklidge JC, Baba N. 1992. Accelerator mass-spectrometric measurements of heavy long-lived isotopes. *Int. J. Radiat. Appl. Instrum. A* 43:279–87
Kilius LR, Rucklidge JC, Litherland AE. 1987. Accelerator mass spectrometry of ^{129}I at isotrace. *Nucl. Instrum. Methods Phys. Res. B* 29:72–76
Köberle C, Gerdes R. 2003. Mechanisms determining the variability of Arctic sea ice conditions and export. *J. Clim.* 16:2843–58
Le Bras I, Straneo F, Muilwijk M, Smedsrud LH, Li F, et al. 2021. How much Arctic fresh water participates in the subpolar overturning circulation? *J. Phys. Oceanogr.* 51:955–73
Livingston HD, Bowen V, Kupferman S. 1982. Radionuclides from Windscale discharges 2: their dispersion in Scottish and Norwegian coastal circulation. *J. Mar. Res.* 40:1227–58
Livingston HD, Jenkins WJ. 1983. Radioactive tracers in the sea. In *Oceanography: The Present and Future*, ed. PG Brewer, pp. 163–91. New York: Springer
Livingston HD, Kupferman SL, Bowen VT, Moore RM. 1984. Vertical profile of artificial radionuclide concentrations in the Central Arctic Ocean. *Geochim. Cosmochim. Acta* 48:2195–203

Annu. Rev. Mar. Sci. 2023.15:203-221. Downloaded from www.annualreviews.org
Access provided by ETH- Zurich on 07/24/23. See copyright for approved use.

Annu. Rev. Mar. Sci. 2023.15:203-221. Downloaded from www.annualreviews.org
Access provided by ETH- Zurich on 07/24/23. See copyright for approved use.

Livingston HD, Povinec PP. 2002. A millennium perspective on the contribution of global fallout radionuclides to ocean science. *Health Phys.* 82:656–68

Livingston HD, Swift JH, Ostlund HG. 1985. Artificial radionuclide tracer supply to the Denmark Strait overflow between 1972 and 1981. *J. Geophys. Res. Oceans* 90:6971–82

Lobelle D, Beaulieu C, Livina V, Sévellec F, Frajka-Williams E. 2020. Detectability of an AMOC decline in current and projected climate changes. *Geophys. Res. Lett.* 47:e2020GL089974

Macdonald RW, Carmack EC. 1991. Age of Canada Basin deep waters: a way to estimate primary production for the Arctic Ocean. *Science* 254:1348–50

Matsumoto K. 2007. Radiocarbon-based circulation age of the world oceans. *J. Geophys. Res. Oceans* 112:C09004

McLaughlin FA, Carmack EC, Williams WJ, Zimmermann S, Shimada K, Itoh M. 2009. Joint effects of boundary currents and thermohaline intrusions on the warming of Atlantic water in the Canada Basin, 1993–2007. *J. Geophys. Res. Oceans* 114:C00A12

Meredith M, Sommerkorn M, Cassotta S, Derksen C, Ekaykin A, et al. 2019. Polar regions. In *IPCC Special Report on the Ocean and Cryosphere in a Changing Climate*, ed. H-O Pörtner, DC Roberts, V Masson-Delmotte, P Zhai, M Tignor, et al., pp. 203–320. Cambridge, UK: Cambridge Univ. Press

Morison J, Kwok R, Peralta-Ferriz C, Alkire M, Rigor I, et al. 2012. Changing Arctic Ocean freshwater pathways. *Nature* 481:66–70

NASA (Natl. Aeronaut. Space Adm.). 2022. Arctic sea ice extent. *NASA*. **https://climate.nasa.gov/vital-signs/arctic-sea-ice**

NCEI (Natl. Cent. Environ. Inf.). 2022. Arctic Oscillation (AO). *NCEI.* **https://www.ncdc.noaa.gov/teleconnections/ao**

Orre S. 2008. *Circulation features in the northern North Atlantic Ocean inferred from simulated radioactive tracers*. PhD Thesis, Univ. Bergen, Bergen, Nor.

Orre S, Smith JN, Alfimov V, Bentsen M. 2010. Simulating transport of ^{129}I and idealized tracers in the northern North Atlantic Ocean. *Environ. Fluid Mech.* 10:213–33

Polyakov IV, Pnyushkov AV, Alkire MB, Ashik IM, Baumann TM, et al. 2017. Greater role for Atlantic inflows on sea-ice loss in the Eurasian Basin of the Arctic Ocean. *Science* 356:285–91

Proshutinsky A, Dukhovskoy D, Timmermans M-L, Krishfield R, Bamber JL. 2015. Arctic circulation regimes. *Philos. Trans. R. Soc. A* 373:20140160

Proshutinsky A, Krishfield R, Timmermans M-L, Toole J, Carmack E, et al. 2009. Beaufort Gyre freshwater reservoir: state and variability from observations. *J. Geophys. Res. Oceans* 114:C00A10

Rabe B, Karcher M, Kauker F, Schauer U, Toole JM, et al. 2014. Arctic Ocean basin liquid freshwater storage trend 1992–2012. *Geophys. Res. Lett.* 41:961–68

Raisbeck GM, Yiou F. 1999. ^{129}I in the oceans: origins and applications. *Sci. Total Environ.* 237–38:31–41

Raisbeck GM, Yiou F, Zhou ZQ, Kilius LR. 1995. ^{129}I from nuclear fuel reprocessing facilities at Sellafield (U.K.) and La Hague (France); potential as an oceanographie tracer. *J. Mar. Syst.* 6:561–70

Rhein M, Kieke D, Steinfeldt R. 2015. Advection of North Atlantic Deep Water from the Labrador Sea to the southern hemisphere. *J. Geophys. Res. Oceans* 120:2471–87

Rudels B. 2009. Arctic Ocean circulation. In *Encyclopedia of Ocean Sciences*, ed. JH Steele, pp. 211–25. Oxford, UK: Academic. 2nd ed.

Rudels B, Anderson L, Eriksson P, Fahrbach E, Jakobsson M, et al. 2012. Observations in the ocean. In *Arctic Climate Change*, ed. P Lemke, HW Jacobi, pp. 117–98. Dordrecht, Neth.: Springer

Sabine CL, Tanhua T. 2010. Estimation of anthropogenic CO_2 inventories in the ocean. *Annu. Rev. Mar. Sci.* 2:175–98

Santschi PH, Schink DR, Corapcioglu O, Oktay-Marshall S, Fehn U, Sharma P. 1996. Evidence for elevated levels of iodine-129 in the Deep Western Boundary Current in the Middle Atlantic Bight. *Deep-Sea Res. I* 43:259–65

Schlitzer R. 1986. ^{14}C in the deep water of the east Atlantic. *Radiocarbon* 28:391–96

Sevellec F, Fedorov AV, Liu W. 2017. Arctic sea-ice decline weakens the Atlantic Meridional Overturning Circulation. *Nat. Clim. Change* 7:604–10

Smethie WM Jr., Fine RA, Putzka A, Jones EP. 2000. Tracing the flow of North Atlantic Deep Water using chlorofluorocarbons. *J. Geophys. Res. Oceans* 105:14297–323

Smith JN, Ellis KM. 1995. Radionuclide tracer profiles at the CESAR Ice Station and Canadian Ice Island in the western Arctic Ocean. *Deep-Sea Res. II* 42:1449–70
Smith JN, Ellis KM, Boyd T. 1999. Circulation features in the central Arctic Ocean revealed by nuclear fuel reprocessing tracers from Scientific Ice Expeditions 1995 and 1996. *J. Geophys. Res. Oceans* 104:29663–77
Smith JN, Ellis KM, Jones EP. 1990. Cesium 137 transport into the Arctic Ocean through Fram Strait. *J. Geophys. Res. Oceans* 95:1693–701
Smith JN, Ellis KM, Kilius LR. 1998. ^{129}I and ^{137}Cs tracer measurements in the Arctic Ocean. *Deep-Sea Res. I* 45:959–84
Smith JN, Jones EP, Moran SB, Smethie WM Jr., Kieser WE. 2005. Iodine 129/CFC 11 transit times for Denmark Strait Overflow Water in the Labrador and Irminger Seas. *J. Geophys. Res. Oceans* 110:C05006
Smith JN, Karcher M, Casacuberta N, Williams WJ, Kenna T, Smethie WM Jr. 2021. A changing Arctic Ocean: how measured and modeled ^{129}I distributions indicate fundamental shifts in circulation between 1994 and 2015. *J. Geophys. Res. Oceans* 126:e2020JC016740
Smith JN, McLaughlin FA, Smethie WM Jr., Moran SB, Lepore K. 2011. Iodine-129, ^{137}Cs, and CFC-11 tracer transit time distributions in the Arctic Ocean. *J. Geophys. Res. Oceans* 116:C04024
Smith JN, Smethie WM Jr., Casacuberta N. 2022. Synoptic ^{129}I and CFC-SF_6 transit time distribution (TTD) sections across the central Arctic Ocean from the 2015 GEOTRACES cruises. *J. Geophys. Res. Oceans* 127:e2021JC018120
Smith JN, Smethie WM Jr., Yashayev I, Curry R, Azetsu-Scott K. 2016. Time series measurements of transient tracers and tracer-derived transport in the Deep Western Boundary Current between the Labrador Sea and the subtropical Atlantic Ocean at Line W. *J. Geophys. Res. Oceans* 121:8115–38
Srokosz MA, Bryden HL. 2015. Observing the Atlantic Meridional Overturning Circulation yields a decade of inevitable surprises. *Science* 348:1255575
Steele M, Boyd T. 1998. Retreat of the cold halocline layer in the Arctic Ocean. *J. Geophys. Res. Oceans* 103:10419–35
Steier P, Bichler M, Fifield KL, Golser R, Kutschera W, et al. 2008. Natural and anthropogenic ^{236}U in environmental samples. *Nucl. Instrum. Methods Phys. Res. B* 266:2246–50
Stöven T, Tanhua T, Hoppema M, Bullister JL. 2015. Perspectives of transient tracer applications and limiting cases. *Ocean Sci.* 11:699–718
Stuiver M. 1980. ^{14}C distribution in the Atlantic Ocean. *J. Geophys. Res. Oceans* 85:2711–18
Swift JH, Jones EP, Aagaard K, Carmack EC, Hingston M, et al. 1997. Waters of the Makarov and Canada basins. *Deep-Sea Res. II* 44:1503–29
Timmermans M-L, Marshall J. 2020. Understanding Arctic Ocean circulation: a review of ocean dynamics in a changing climate. *J. Geophys. Res. Oceans* 125:e2018JC014378
Toole JM, Andres M, Le Bras IA, Joyce TM, McCartney MS. 2017. Moored observations of the Deep Western Boundary Current in the NW Atlantic: 2004–2014. *J. Geophys. Res. Oceans* 122:7488–505
Waugh DW, Hall TM. 2005. Propagation of tracer signals in boundary currents. *J. Phys. Oceanogr.* 35:1538–52
Waugh DW, Hall TM, Haine TWN. 2003. Relationships among tracer ages. *J. Geophys. Res. Oceans* 108:3138
Wefing A-M, Casacuberta N, Christl M, Gruber N, Smith JN. 2021. Circulation timescales of Atlantic Water in the Arctic Ocean determined from anthropogenic radionuclides. *Ocean Sci.* 17:111–29
Wefing A-M, Christl M, Vockenhuber C, Rutgers van der Loeff M, Casacuberta N. 2019. Tracing Atlantic waters using ^{129}I and ^{236}U in the Fram Strait in 2016. *J. Geophys. Res. Oceans* 124:882–96
Woodgate R. 2013. Arctic Ocean circulation: going around at the top of the world. *Nat. Educ. Knowl.* 4:8
Yiou F, Raisbeck GM, Zhou ZQ, Kilius LR. 1994. ^{129}I from nuclear fuel reprocessing; potential as an oceanographic tracer. *Nucl. Instrum. Methods Phys. Res. B* 92:436–39

Annu. Rev. Mar. Sci. 2023.15:203-221. Downloaded from www.annualreviews.org
Access provided by ETH- Zurich on 07/24/23. See copyright for approved use.

Annual Review of Marine Science

Volume 15, 2023

Contents

Annu. Rev. Mar. Sci. 2023.15:203-221. Downloaded from www.annualreviews.org
Access provided by ETH - Zurich on 07/24/23. See copyright for approved use.

Errata

An online log of corrections to *Annual Review of Marine Science* articles may be found at http://www.annualreviews.org/errata/marine

Annu. Rev. Mar. Sci. 2023.15:203-221. Downloaded from www.annualreviews.org
Access provided by ETH- Zurich on 07/24/23. See copyright for approved use.